Reprinted from
Journal of Imaging Science and Technology® 64(5): 050408-1–050408-9, 2020.

Spectral Estimation of Multiple Light Sources based on Highlight Detection

Shoji Tominaga▲
Department of Computer Science, Norwegian University of Science and Technology, 2815 Gjøvik, Norway
Department of Business and Informatics, Nagano University, Ueda 386-1298, Japan
E-mail: shoji-tominaga@nagano.ac.jp

Keita Hirai▲ **and Takahiko Horiuchi**▲
Department of Imaging Sciences, Chiba University, Chiba 263-8522, Japan

Abstract. *The authors discuss the spectral estimation of multiple light sources from image data in a complex illumination environment. An approach is proposed to effectively estimate illuminant spectra and the corresponding light sources based on highlight areas that appear on dielectric object surfaces. First, the authors develop a highlight detection method using two types of convolution filters with Gaussian distributions, center-surround and low-pass filters. This method is available even for white surfaces, and it is independent of object color and of viewing and incidence angles. Second, they present an algorithm for estimating the illuminant spectra from extracted highlight areas. Each specular highlight area has a spectral composition corresponding to only one light source among multiple light sources. The spectral image data are projected onto a two-dimensional subspace, where a linear cluster in pixel distribution is detected for each highlight area. Third, the relative positional relationship between highlight areas among different object surfaces is used to identify the light sources on each surface. The authors develop an algorithm based on probabilistic relaxation labeling. The light source for each highlight and the corresponding spectral-power distribution are determined from the iterative labeling process. Finally, the feasibility of the proposed approach is examined in an experiment using a real complex environment, where dielectric objects are illuminated by multiple light sources of light-emitting diode, fluorescence, and incandescence.* © *2020 Society for Imaging Science and Technology.*
[DOI: 10.2352/J.ImagingSci.Technol.2020.64.5.050408]

1. INTRODUCTION

The estimation of scene illumination from imaging data has essential applications in a variety of fields, including image rendering, material appearance, color constancy, image processing, computer vision, and illumination design. For instance, we judge the appearance of an object using the light reflected from that object and nearby objects. The spectral composition of this reflected light, sometimes called the color signal, depends on the surface reflectance of objects and the spectral composition of the illuminating light. If the illuminant spectrum and the surface-spectral reflectance for a non-metallic material such as a dielectric material are estimated, we can render the color image to realize the appearance of the same material under different illuminants. Humans have some ability to discount illumination when judging object appearance. This ability, called color constancy, demonstrates at least a subconscious ability to separate the illuminant spectral-power distribution from the surface reflectance function within the color signal [1]. Computational color constancy discussed in computer vision tries to maintain stable color appearance across light sources, and using the estimated illuminant, the captured image is corrected so that it appears to be taken under a standard (e.g., white) light source. When we change the illumination environment in a real scene, we have to first know the illuminant spectral-power distributions and the spatial distributions of light sources existing in the scene.

The scene illuminant estimation problem has a long history. Although so far, many methods have been proposed for scene illuminant estimation, most methods assumed uniform illumination from a single light source [2–4]. We note that our illumination environment is not necessarily a single light source such as daylight or a light bulb, but it often consists of multiple light sources from different directions (e.g., see [5, 6]). The case of one source seldom occurs.

This article discusses the problem of estimating light sources and their spectral-power distributions from the spectral image data of objects acquired in a complex illumination environment. The target objects are everyday objects, which are usually assumed to be made of an inhomogeneous dielectric material such as plastic, ceramic, or paint. Imai et al. [7] discussed three specular highlight detection methods: (1) use of variable thresholding of luminance, (2) use of luminance and hue components, and (3) use of a polarization filter. Among these, (1) was based on recursive thresholding of luminance histograms, (2) had difficulty in detecting highlight on white object surfaces because of using hue, and (3) had the problem of instability of detection because the polarization degree depends significantly on the angle of incidence to the object surface. Tominaga et al. [8] discussed the relative positional relationship of multiple light sources based on highlight detection. Koirala et al. [9] proposed a highlight detection method with a strong constraint under a single illuminant. It is an essential problem that what we perceive as a highlight

▲ IS&T Members.

Received May 27, 2020; accepted for publication Aug. 1, 2020; published online Sep. 4, 2020. Associate Editor: Michael Murdoch.
1062-3701/2020/64(5)/050408/9/$25.00

is not based on the absolute value of the light intensity, but this is based on relative contrast. Therefore, the brighter part, even with a dark object color, is regarded as the highlight. The highlight perception also depends on the object color.

In the present article, first, we propose a direct and compact highlight detection method by taking a human visual system into account. When our visual system perceives the appearance of an object, we can quickly recognize texture and gloss on the surface. In our vision system, incoming light is detected by cells such as retinal ganglion cells with a center-surround-type visual field. All of the receptive fields have an excitatory center and an inhibitory surround. This detection can be well described as the difference between two Gaussian distributions: a narrower positive Gaussian and a broader negative Gaussian (see [1]). We can use this filtering as the first step for highlight detection. We consider that the filter output is mostly unaffected by the object color since the filtering is based on the difference between two Gaussian distributions. An additional filtering operator is also devised for detecting boundary regions between different objects to improve highlight detection.

Second, we estimate the spectral-power distributions for the detected highlight areas. The object surface made of dielectric material possesses the dichromatic reflection property that light reflection is a linear sum of the specular component and the diffuse component. Since the specular component has the same spectral composition as the light source, most notably, the highlight area contains illuminant spectral information. Therefore, we present an algorithm for estimating the illuminant spectrum from the extracted highlight areas. We note that when the surface is convex, each of the detected highlight areas corresponds to only one light source among multiple light sources. The captured spectral image data at each highlight area are projected onto a two-dimensional subspace. Thus, illuminant estimation is reduced to the detection of the linear cluster in the two-dimensional subspace. The illuminant spectral curve can be estimated by the principal-component analysis of each highlight pixel distribution.

Third, the estimated spectral curves from the highlights on different object surfaces must uniquely correspond to the light sources existing in different spatial places. We use the relative positional relationship between highlight areas among different object surfaces to identify the light sources on each surface. An algorithm based on probabilistic relaxation labeling is developed for reasonable labeling of the highlights. The light source for each highlight and the corresponding spectral-power distribution are determined from the iterative labeling process.

Finally, the feasibility of the proposed approach is examined in an experiment using a real complex environment, where dielectric objects are illuminated by multiple light sources of light-emitting diode (LED), fluorescence, and incandescence. We show the effectiveness of the highlight detection method and the accuracy of the identified light sources and their illuminant spectra based on the highlights.

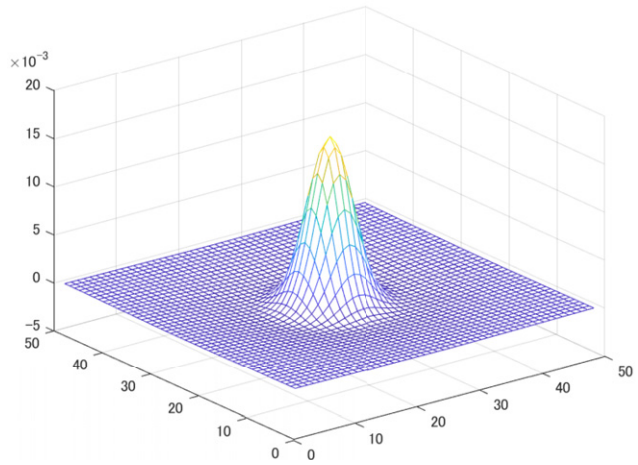

Figure 1. Filter shape of the center surround with $\sigma_1 = 3$ and $\sigma_2 = 12$.

2. HIGHLIGHT DETECTION

Let $Y(\lambda)$ be the observed color signal (spectral radiance of the reflected light) from an object surface at each pixel point. The color signals can be recovered from the outputs of the spectral imaging system by knowing the spectral sensitivity functions. A discrete form of the color signal is often represented as an n-dimensional column vector when the visible range (400–700 nm) is sampled at n wavelengths with equal intervals. Typically, in this article, all spectral computations are carried out in a high dimension of $n = 61$ with 5 nm intervals. First, we calculate the luminance value L of the color signals as

$$L = \int_{400}^{700} Y(\lambda)\overline{y}(\lambda)d\lambda, \tag{1}$$

where $\overline{y}(\lambda)$ is the CIE luminosity function.

The kernel of a Gaussian filter is described as

$$G(x, y, \sigma) = \frac{1}{2\pi\sigma^2}\exp\{-(x^2 + y^2)/(2\sigma^2)\}, \tag{2}$$

where (x, y) are variables of the two-dimensional array and σ is the standard deviation of the Gaussian distribution. A filter creating a center-surround field is determined by a difference of two Gaussian distributions of equal areas. Let σ_1 and σ_2 be the standard deviations with $\sigma_2 > \sigma_1$. Then the broader Gaussian is subtracted from the narrower Gaussian as $G(x, y, \sigma_1) - G(x, y, \sigma_2)$. The filter outputs applied to the luminance image L are calculated by a convolution

$$Z_1 = L * G(x, y, \sigma_1) - L * G(x, y, \sigma_2). \tag{3}$$

Since the kernel is usually expressed using a matrix, the convolution is carried out by multiplying pixel values of the luminance image by the matrix over some range.

Figure 1 shows the filter shape with $\sigma_1 = 3$ and $\sigma_2 = 12$. We applied this filter to an example image shown in Figure 2. Figure 3(a) is the filter output image, and Fig. 3(b) is the resulting image after simple thresholding. We see in Fig. 3(b) that the specular highlight areas are well detected in yellow and green while a boundary region between the object and

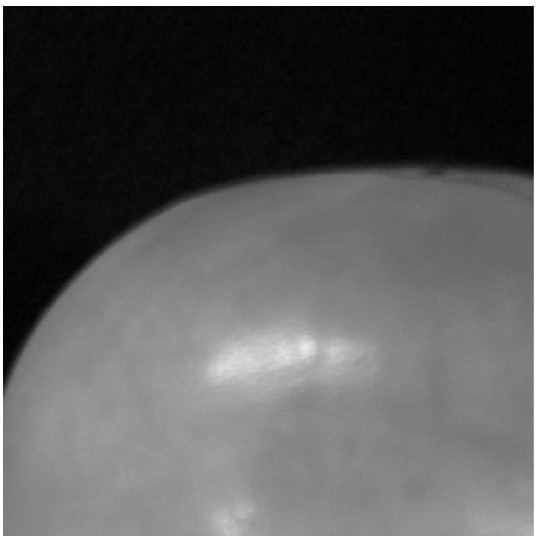

Figure 2. Example image of a simple object.

the background is detected in blue. The filter enhances the big luminance difference in the boundary. Therefore, we devise a separate filtering operator for detecting boundary regions. The second filter is described as $G(x, y, \sigma_3) - 1$, and the filter outputs to the image are described as

$$Z_2 = L * G(x, y, \sigma_3) - L, \tag{4}$$

where $\sigma_3 > \sigma_2$. This filter is a low-pass filter for operating over a wide range so that the outside of the boundary is detected. Figure 4 shows the filter shape with $\sigma_3 = 15$. Figure 5(a) is the filter output image, and Fig. 5(b) is the resulting image after simple thresholding. The boundary region is detected in yellow. Now we know which of the detected areas in Fig. 3(b) belongs to the boundary. Thus, a set of highlight areas is determined by removing the boundary areas from the set of areas detected by the above Gaussian filter.

3. ILLUMINANT ESTIMATION

The detected highlight areas provide an important clue for estimating the light sources. We note that even though multiple light sources illuminate a convex object surface from different directions, each of the highlight areas corresponds to a single light source. Figure 6 shows a relationship between a camera and multiple light sources illuminating a convex object surface. When an object possesses the dichromatic reflection property, the reflected light is composed of a diffuse reflection component and a specular reflection component. The specular reflection component produces a highlight with a strong luminance value. Specular reflection occurs only when the incidence angle of the incoming light is coincident with the viewing angle by a camera. In other words, the highlight occurs only on the portion of the surface where the viewing angle agrees with the incidence angle of light. Therefore, each of the detected highlight areas contains the illuminant information of the corresponding only one light source among multiple light sources.

The observed color signal from an inhomogeneous dielectric object is described by the dichromatic reflection model as follows:

$$Y(\lambda) = Y_D(\lambda) + Y_S(\lambda), \tag{5}$$

where the suffixes D and S indicate the diffuse reflection component and the specular reflection component, respectively. To express the model in terms of surface reflectance and the illuminant, let $S_S(\lambda)$ be the surface-spectral reflectance of the target object and let $E(\lambda)$ be the spectral-power distribution of the incident light. Thus, the color signal observed at a highlight area is described as

$$Y(\lambda) = S_S(\lambda)E(\lambda) + CE_i(\lambda), \tag{6}$$

where $E(\lambda)$ is the mixture of different illuminant spectra from N light sources of $E(\lambda) = E_1(\lambda) + E_2(\lambda) + \cdots + E_N(\lambda)$, $E_i(\lambda)$ is the illuminant spectrum of a single light source corresponding to the highlight, and C is a constant over the visible wavelength range. The present problem is to estimate $E_i(\lambda)$ based on the data set of observed color signals $\{Y(\lambda)\}$.

For computational convenience, we use discrete representation in spectral analysis. Let $\mathbf{y}$ be an n-dimensional vector of the color signal $Y(\lambda)$ observed by a spectral imaging system. Because of the two-dimensionality of $\mathbf{y}$, the image data with high dimension in each highlight area are projected onto a two-dimensional subspace spanned by two principal components. The component vectors $\mathbf{p}_1$ and $\mathbf{p}_2$ are computed as the first and second principal components of the data set $\{\mathbf{y}\}$. We can derive the mapping equation

$$\begin{bmatrix} c_1 \\ c_2 \end{bmatrix} = \begin{bmatrix} \mathbf{p}_1{}^t \\ \mathbf{p}_2{}^t \end{bmatrix} \mathbf{y}. \tag{7}$$

Figure 7 shows an example of pixel distribution (histogram) of the image data in a highlight area projected on the two-dimensional subspace. Although the pixel distribution appears as a straight line, it consists of two clusters. The pixel distribution on the upper right in the figure mostly belongs to the diffuse cluster, and the remaining linear distribution is the cluster by the specular reflection component. The directional vectors of this linear cluster correspond to the light source color, that is, the illuminant to be estimated. We note that the linear highlight cluster is much longer than the diffuse cluster. In this article, we extract the directional vector of the highlight cluster in a simple way as follows. First, the centroid A of the pixel distribution is calculated, and the farthest pixel point B from the centroid is detected as shown in Fig. 7(a). Second, the boundary point C is set to a position slightly shifted from the center of gravity toward the farthest point. The pixels along the straight line from C to B are selected again as a specular cluster as shown in Fig. 7(b). Then the first principal-component vector of this specular cluster is extracted, and its direction vector is determined.

Let the directional vector be (c_1', c_2'). Then, the illuminant vector $\mathbf{E}$ can be estimated by transforming (c_1', c_2')

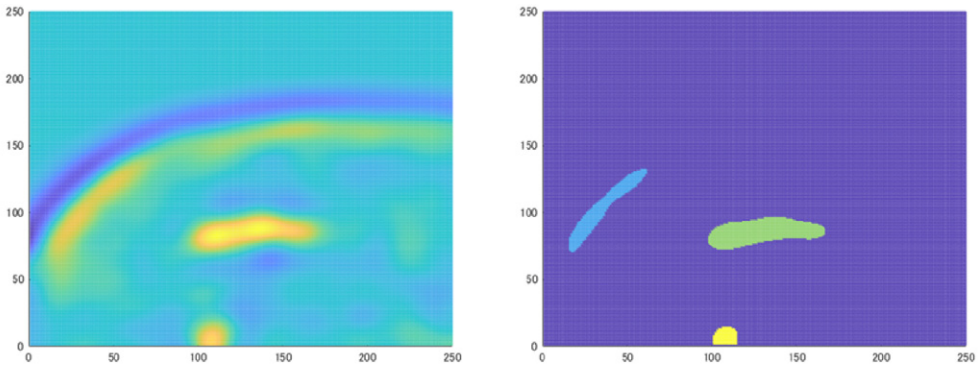

Figure 3. Filtering results for the image from Figure 1. (a) Filter output image. (b) Image after simple thresholding.

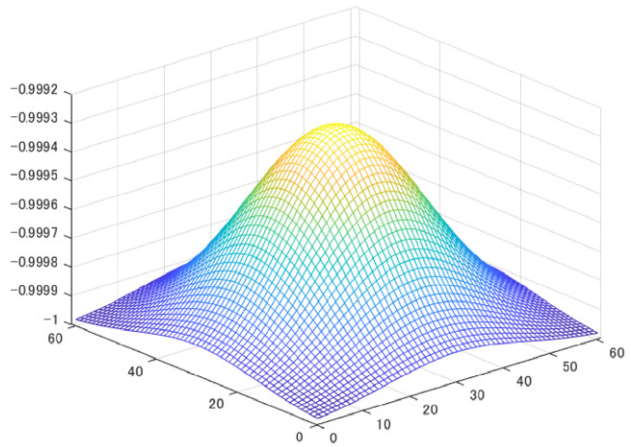

Figure 4. Filter shape of the boundary detection with $\sigma_3 = 15$.

inversely into the high-dimensional spectral space as follows:

$$\hat{\mathbf{E}} = \begin{bmatrix} \mathbf{p}_1{}^t \\ \mathbf{p}_2{}^t \end{bmatrix}^+ \begin{bmatrix} c_1' \\ c_2' \end{bmatrix}, \tag{8}$$

where the symbol $+$ indicates the generalized inverse of the matrix. We obtain the estimates of the illuminant spectra from the respective highlight areas.

Let $\{\hat{\mathbf{E}}_1, \hat{\mathbf{E}}_2, \ldots, \hat{\mathbf{E}}_M\}$ be a set of estimated illuminant spectra from M highlight areas. Since the estimates contain errors, we classify the estimated spectral curves into several groups to find a reliable set of illuminant estimates. We adopt the K-means clustering algorithm [10] for performing this grouping. The algorithm has an iterative process. It starts with initial estimates for the K centroids of illuminants, which are randomly selected from the spectral data set or as random numbers, where each centroid defines one of the clusters. Second, each data point is assigned to its nearest centroid based on the Euclidean distance. The centroid is then recalculated in each cluster.

It should be noted that unless the number M of highlights is large, the classification result depends largely on the initial values. Therefore, we repeat the clustering algorithm by changing the initial values randomly. If the number N of light sources is known in advance, then we set K to N.

4. IDENTIFICATION OF HIGHLIGHT LOCATIONS AND LIGHT SOURCES

Classification using the estimated spectra is not sufficient to identify the light sources on each object surface. When specular highlights appear on multiple objects in the scene, we have to assign the most matching illuminant to each of the detected highlight locations on each object surface. When the object surfaces are convex, the detected highlights on each object surface correspond to different light sources. Note that in this case, the highlight locations on each surface are closely related to the directions relative to where those light sources exist. For example, the highlight position on the left suggests that the light source is located left, and the light comes from the left direction. Similarly, the highlight positions on the top and right suggest illuminations coming from the upper and right directions, respectively. Thus, the relative positional relationship between highlight areas among different object surfaces is useful for the identification of spectral light sources on each surface. We use not only the illuminant spectral information but also the highlight locational information. The method of probabilistic relaxation labeling (e.g., see [11–14]) is applied to solving the present identification problem.

Figure 8 depicts an example showing positional relationship between highlight positions on two object surfaces. Let label L_k be the kth highlight on a reference object that has the most highlights among all the objects. Let O_i be the ith highlight on another object. The detection of the relative positional relationship involves finding the most matching highlight label L_{k*} on the reference object for all highlights $\{O_i\}$ on the other object. The probabilistic relaxation gives highlight O_i a probability P_{ik} ($\sum_k P_{ik} = 1$) for each label L_k on the reference object. In Fig. 8, P_{13} shows the probability that the highlight O_1 matches the highlight L_3.

A candidate label, L_{k*}, with the maximum probability is assigned as the final corresponding highlight for highlight O_i. The initial probabilities are derived from the root-mean-square error, $\mathrm{RMSE}_{ik} = \|\hat{\mathbf{E}}_i - \hat{\mathbf{E}}_k\|^{1/2}$, of the estimated

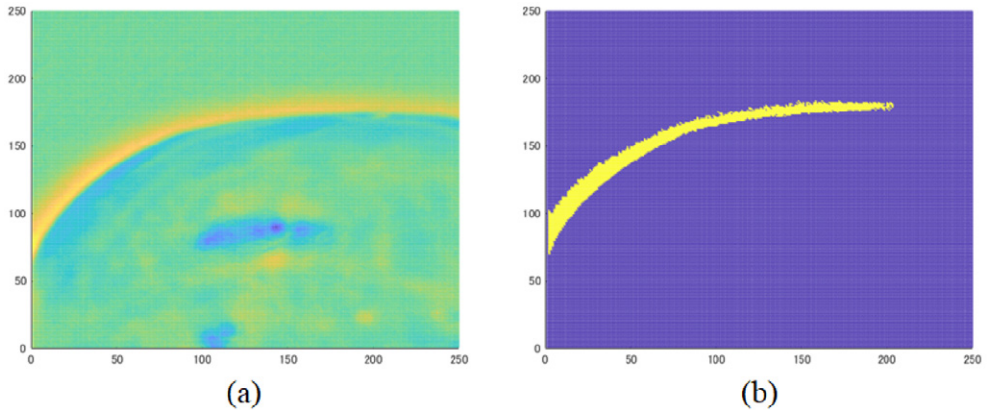

Figure 5. Filtering results by using the filter in Figure 4. (a) Filter output image. (b) Image after simple thresholding.

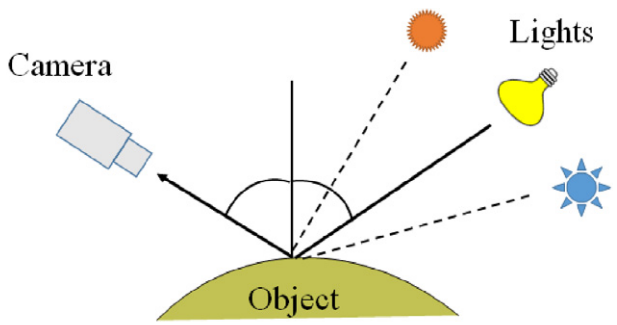

Figure 6. Relationship between a camera and multiple light sources illuminating a convex surface.

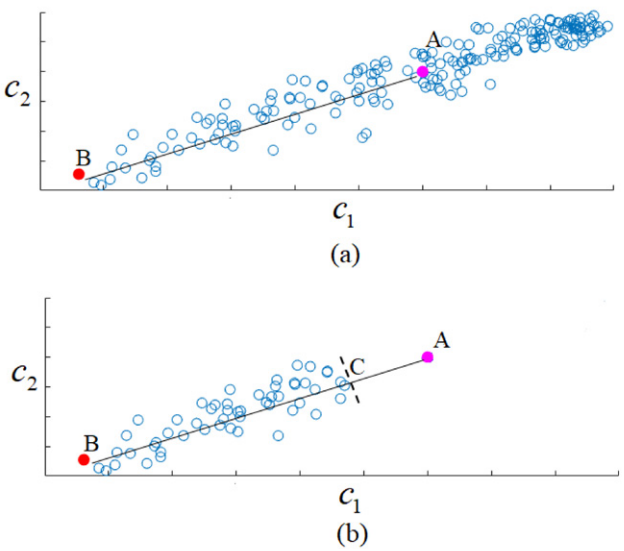

Figure 7. Pixel distribution of the image data in a highlight area projected on the two-dimensional space (c_1, c_2).

spectral-power distributions between L_k and O_i as

$$P_{ik}^{(0)} = \frac{1/\mathrm{RMSE}_{ik}}{\sum_{k'}(1/\mathrm{RMSE}_{ik'})}. \tag{9}$$

In the special case where two spectral-power distributions are coincident as $\mathrm{RMSE}_{ik} = 0$, the initial probability may be modified by an appropriate positive number ε as

$$P_{ik}^{(0)} = \frac{1/\max(\mathrm{RMSE}_{ik}, \varepsilon)}{\sum_{k'}(1/\max(\mathrm{RMSE}_{ik'}, \varepsilon))}. \tag{10}$$

Then, the iterative processing is started, and the probabilities are updated by the following iterative equation:

$$P_{ik}^{(t+1)} = \frac{P_{ik}^{(t)} \times q_{ik}^{(t)}}{\sum_{k'}(P_{ik'}^{(t)} \times q_{ik'}^{(t)})}. \tag{11}$$

The compatibility function (CF) denotes the contribution from the other highlights, which are defined as follows:

$$q_{ik}^{(t)} = \sum_j \{\max_l (r_{ijkl} \times P_{jl}^{(t)})\}, \tag{12}$$

where L_l and O_j are the labels for highlight l on the reference object and highlight j on another object, respectively. The CF evaluates only the candidate label with the maximum probability. Compatibility coefficients, r, are formulated as follows:

$$r_{ijkl} = \max(0, \alpha - \Delta\mathrm{deg}_{ijkl}), \quad (\alpha > 0), \tag{13}$$

where Δdeg indicates the spatial relationship between a pair of target highlights $\{L_k, O_i\}$ and another pair of highlights $\{L_l, O_j\}$. The quantity Δdeg is calculated using the angular difference deg_{ij}[rad] for a segment from i to j and the angular difference deg_{kj} [rad] for a segment from k to l as

$$\Delta\mathrm{deg}_{ijkl} = \begin{cases} |\mathrm{deg}_{kl} - \mathrm{deg}_{ij}|, & |\mathrm{deg}_{kl} - \mathrm{deg}_{ij}| \le \pi \\ 2\pi - |\mathrm{deg}_{kl} - \mathrm{deg}_{ij}|, & |\mathrm{deg}_{kl} - \mathrm{deg}_{ij}| > \pi \end{cases}. \tag{14}$$

The iterative process is convergent if the following condition is satisfied,

$$\left| \max_k P_{ik}^{(t+1)} - \max_k P_{ik}^{(t)} \right| < Th, \forall O_i, \tag{15}$$

where Th represents the threshold of the convergence condition. Then, the label L_{k*} with the maximum probability

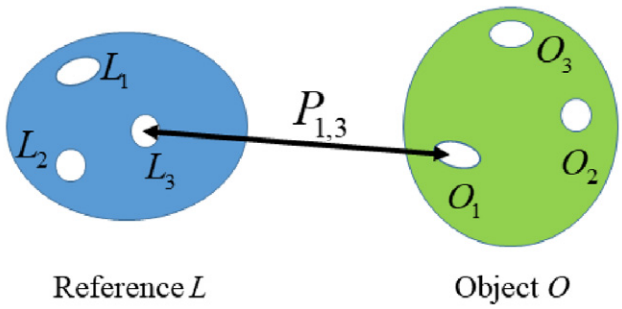

Figure 8. Example showing the positional relationship between highlight positions on two object surfaces.

$P_{ik}^{(t)}$ is assigned as the final corresponding highlight for highlight O_i.

After performing the above computational process for all objects, a set of corresponding highlights on all objects is determined for each label highlight L_k on the reference object. If the corresponding highlights are empty for a label highlight, we remove the label highlight as a wrongly selected highlight. The number of the label highlight on the reference object becomes the number of light sources. The light source and its spectral-power distribution are determined by the relative positional relationship of the highlights to the reference object.

5. EXPERIMENTAL RESULTS

5.1 *Spectral Imaging System*

A spectral imaging system was used in experiments, which consisted of a monochrome charge-coupled device camera with 12-bit dynamic range and Peltier cooling (QImaging, Retiga 1300), a VariSpec liquid crystal tunable filter, an infrared-cut filter, and a personal computer [15]. The spectral images were captured at 5 nm intervals in the visible wavelength range. Thus, each captured image was represented in an array of 61-dimensional vectors.

We created a complex illumination environment in an indoor scene using three different light sources: (1) incandescent light source from a light bulb, (2) fluorescent light source from a table lamp, and (3) LED light source from a ceiling lamp. Figure 9 shows the spectral-power distributions for the three light sources.

The target objects were selected from everyday products we usually see. Figure 10 shows a color image of the captured image, including three objects under multiple illuminations, where the left object is made of real ceramic and the center and right objects are a persimmon and an apple, which are not natural but artificial. These objects were illuminated by the incandescent light from the left, the LED from above, and the fluorescent light from the right.

5.2 *Detection of Highlight Areas*

The spectral image captured from the scene was converted into a luminance image to which the proposed filters were applied. Figure 11 shows the filtration outputs by the center-surround filter, with $\sigma_1 = 3$ and $\sigma_2 = 12$, and the candidate highlight areas extracted by thresholding.

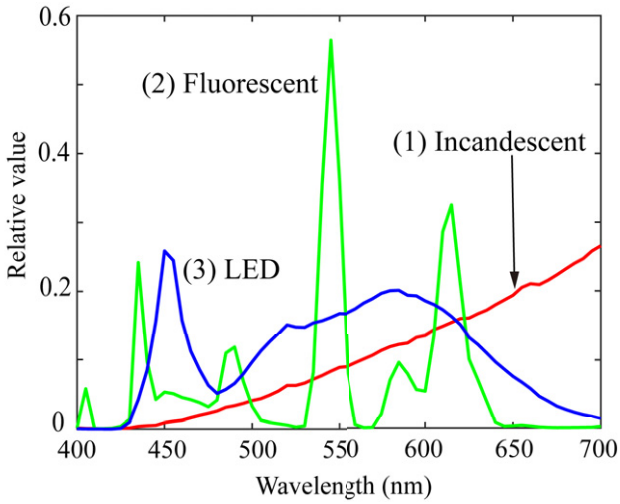

Figure 9. Spectral-power distributions for the three light sources used in experiments.

Figure 10. Color image of the captured image for the three objects under different illuminations.

Two strong and sharp specular highlight areas on the ceramic object are clearly extracted as shown in Fig. 11(a). Figure 12 shows the boundary detection result by the proposed low-pass filter in Eq. (4) with $\sigma_3 = 40$. We note that the outside of the boundary between the objects and the background is detected. Each candidate highlight area in Fig. 11(b) was examined whether it belonged to any boundary regions, and specular highlight areas except for the boundary were left. The detected area located leftmost on the

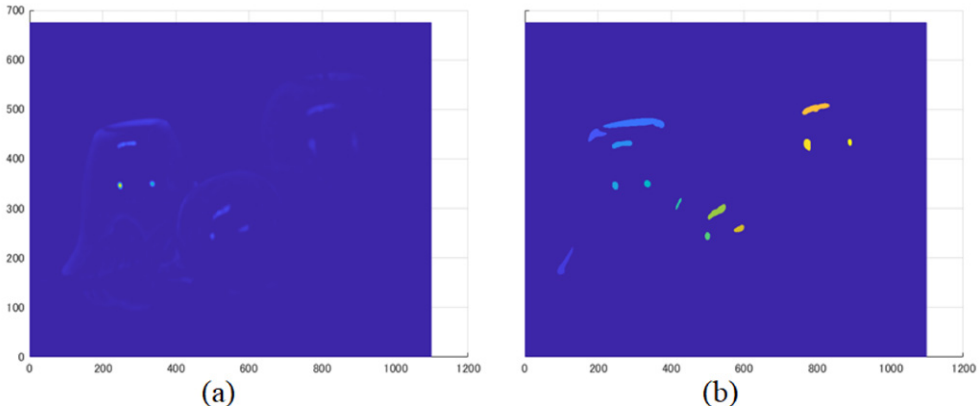

Figure 11. Filtration result for the captured image by the center-surround filter: (a) output image and (b) candidate highlight areas extracted by thresholding.

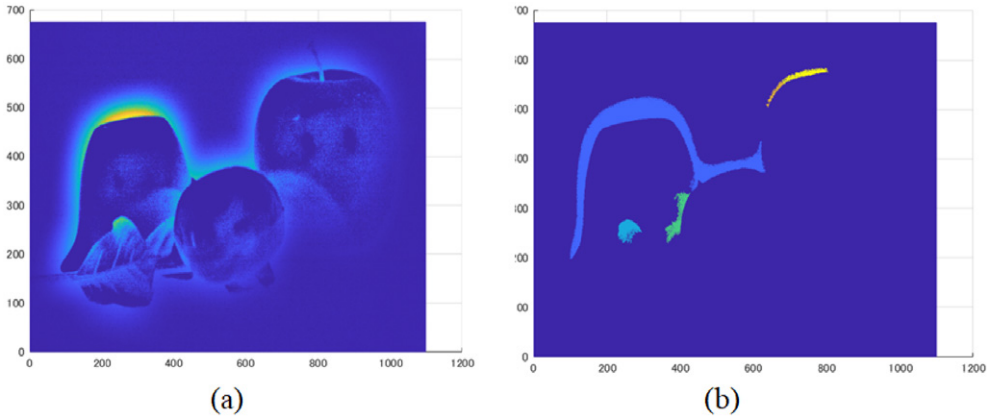

Figure 12. Boundary detection result by the low-pass filter (Eq. (4)): (a) filter output image and (b) detected boundary regions.

Figure 13. Whole set of nine highlight areas detected from the captured image of the three objects.

ceramic object was overlooked in this process; so we removed it manually. Figure 13 depicts the whole set of nine highlight areas extracted from the three object surfaces.

5.3 *Illuminant Estimation*

The spectral-power distribution was estimated for each of the detected highlight areas. The singular value decomposition was applied to the data set {y} of the observed spectra at each highlight area. The spectral data were then mapped onto a plane defined by two principal-component vectors. If the specular reflection in the highlight area is much stronger compared with the diffuse reflection, the pixel distribution consists of an almost specular cluster and takes a linear shape. Most highlight areas exhibited linear clusters as shown in Fig. 7. The illuminant spectra were estimated along with the proposed algorithm. The area of the ceramic object was overlooked in the previous detection, stage B. This area can be removed at the illuminant estimation stage because the first principal component of that area has the same spectral composition as the diffuse reflection on the yellow ceramic object. Thus, that area is not a specular highlight area but a diffuse reflection area with the object color.

Figure 14 shows a set of estimated illuminant spectra $\{\hat{\mathbf{E}}_1, \hat{\mathbf{E}}_2, \ldots, \hat{\mathbf{E}}_9\}$ from nine highlight areas. These spectral curves were then classified into several classes. We applied the K-means clustering algorithm to these spectral curves. The algorithm was repeatedly executed 1000 times while randomly changing the initial values. For $K = 3$, the estimated spectral curves are classified into three classes as follows:

$$\hat{\mathbf{E}}_1{:}3,\ \hat{\mathbf{E}}_2{:}1,\ \hat{\mathbf{E}}_3{:}2,\ \hat{\mathbf{E}}_4{:}1,\ \hat{\mathbf{E}}_5{:}1,\ \hat{\mathbf{E}}_6{:}2,\ \hat{\mathbf{E}}_7{:}3,\ \hat{\mathbf{E}}_8{:}1,\ \hat{\mathbf{E}}_9{:}2,$$

where the first class corresponds to incandescent light and the second and third classes correspond to fluorescent light

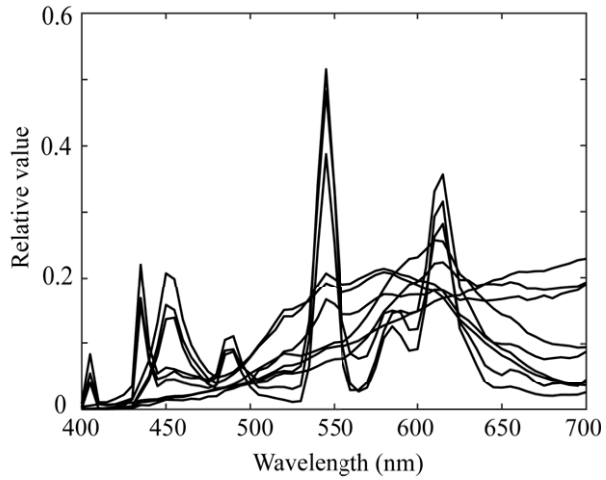

Figure 14. Set of estimated illuminant spectra from nine highlight areas.

and LED, respectively. Therefore, the fifth highlight $\hat{\mathbf{E}}_5$ appears misclassified into the first class.

5.4 *Illuminant Identification Based on Highlight Locations*

Since each of the three object surfaces has three highlights, we cut out a region containing three highlights from each object image as shown in Figure 15. In the figure, Objects 1, 2, and 3 correspond to the left, center, and right objects in the scene of Fig. 13, respectively, and the red point represents the relative coordinates of the center position for each highlight area. We specify Object 1 as the reference object, and Objects 2 and 3 as the target objects. The initial probabilities are as follows:

$$\boldsymbol{P}^{(0)}(2,1) = \begin{bmatrix} 0.171 & 0.699 & 0.130 \\ 0.415 & 0.366 & 0.219 \\ 0.262 & 0.252 & 0.487 \end{bmatrix},$$

$$\boldsymbol{P}^{(0)}(3,1) = \begin{bmatrix} 0.765 & 0.117 & 0.117 \\ 0.241 & 0.593 & 0.167 \\ 0.209 & 0.145 & 0.646 \end{bmatrix},$$

where $\boldsymbol{P}(m,n)$ represents the matrix of $\boldsymbol{P}_{ik}$ for the target object m and the reference object n. After seven iterations ($t=7$) of the proposed probabilistic relaxation labeling, the iterative process converges as

$$\boldsymbol{P}^{(7)}(2,1) = \begin{bmatrix} 0.000 & 1.000 & 0.000 \\ 1.000 & 0.000 & 0.000 \\ 0.000 & 0.000 & 1.000 \end{bmatrix},$$

$$\boldsymbol{P}^{(7)}(3,1) = \begin{bmatrix} 1.000 & 0.000 & 0.000 \\ 0.000 & 1.000 & 0.000 \\ 0.000 & 0.000 & 1.000 \end{bmatrix},$$

where $\alpha = 2$. Therefore, we determine that the highlight spectra $\{\hat{\mathbf{E}}_1, \hat{\mathbf{E}}_5, \hat{\mathbf{E}}_7\}$, $\{\hat{\mathbf{E}}_2, \hat{\mathbf{E}}_4, \hat{\mathbf{E}}_8\}$, and $\{\hat{\mathbf{E}}_3, \hat{\mathbf{E}}_6, \hat{\mathbf{E}}_9\}$ belong to three different classes. Each class has the same light sources. Figure 16 plots the spectral curves averaged within the respective classes. We can see that the first (red), second (green), and third (blue) curves correspond, respectively, to the illuminant spectra of incandescent, fluorescent, and LED light sources. The dashed curves in Fig. 16 show the original illuminant spectral-power distributions in Fig. 9 for comparison. The root-mean-square errors between the estimated and original spectral curves are 0.011, 0.017, and 0.011 for the respective light sources. Thus, we conclude that the objects are illuminated by LED light, incandescent light, and fluorescent light from the upper, left, and right directions, respectively.

6. CONCLUSIONS

In this article, we have discussed the illuminant estimation of multiple light sources from image data under a complex illumination environment. Objects made of an inhomogeneous dielectric material like plastic, ceramic, or paint were used for the illuminant estimation. We developed an approach to adequately estimate the illuminant spectra based on highlight areas appearing on the object surfaces.

First, we proposed a direct and compact highlight detection method. Highlight areas were detected using two types of convolution filters with Gaussian distributions, center-surround and low-pass filters. This method has such excellent features that it is available even for white surfaces, and it is independent of object color and of viewing and incidence angles.

Second, we presented an algorithm for estimating the illuminant spectrum from the extracted highlight areas. Light reflection of each object was a linear sum of the specular component and the diffuse component. Specular reflection has the same spectral composition as a light source. Therefore, we found that each of the detected highlight areas contained the illuminant information of the corresponding only one light source among multiple light sources. The high-dimensional spectral data were projected onto a two-dimensional subspace, where the pixel distribution was divided into two clusters. For the highlight area, the pixel distribution was mainly a linear cluster by specular reflection. Thus, illuminant estimation was reduced to the detection of the linear cluster, and the illuminant spectral curve was estimated from each highlight area.

Third, the spectral curves estimated from the highlights on different object surfaces must uniquely correspond to the light sources existing in different spatial places. The relative positional relationship between highlight positions among different object surfaces was useful to identify the light sources on each surface. We developed an algorithm based on probabilistic relaxation labeling for this purpose. The light source for each highlight and the corresponding spectral-power distribution were determined from the iterative labeling process.

We performed an experiment to examine the feasibility of the proposed approach using three objects made of dielectric and an actual complex environment with multiple light sources of LED, fluorescence, and incandescence. We showed the effectiveness of the proposed highlight detection

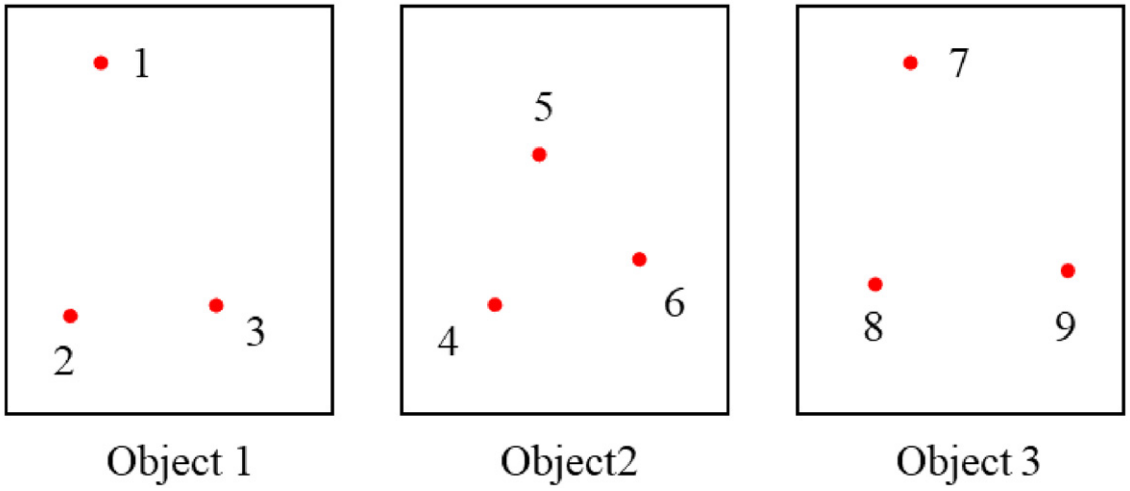

Figure 15. Regions containing three highlights cut out from each object image, where Objects 1, 2, and 3 correspond to the left, center, and right objects in the scene, respectively. The red point represents the relative coordinates of the center position for each highlight area.

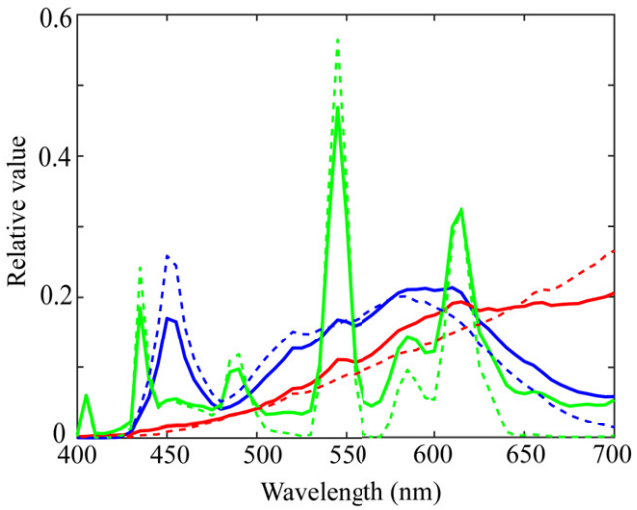

Figure 16. Spectral curves averaged within the respective classes, where three bold curves correspond to the illuminant spectra of incandescent, fluorescent, and LED light sources. The dashed curves represent the original illuminant spectral-power distributions.

method and the accuracy of the estimated illuminant spectra based on the highlights. We note that the relative positional relationship of multiple light sources can be known.

The choice of objects plays a role when diffuse reflection is significant. Our approach cannot be used for objects consisting of only diffuse reflection or for pure matte surface. Our method has the constraint that object surfaces are made of dielectric material with the dichromatic reflection property. The accuracy of illuminant estimation improves as the number of highlight areas and the intensity of the highlight increase. If the highlight areas include the mutual illumination effect from adjacent object surfaces, the highlight areas should be neglected in the estimation. Our approach has the geometric constraint that the object surfaces to be analyzed in a scene are convex.

ACKNOWLEDGMENT

This work was supported by the Japan Society for the Promotion of Science (JSPS) (15H05926).

REFERENCES

[1] B. A. Wandell, *Foundations of Vision* (Sinauer Associates, Sunderland, MA, 1995).
[2] S. Tominaga and B. A. Wandell, "Natural scene illuminant estimation using the sensor correlation," Proc. IEEE **90**, 42–56 (2002).
[3] S. D. Hordley, "Scene illuminant estimation: Past, present and future," Color Res. Appl. **31**, 303–314 (2006).
[4] H. A. Khan, J. B. Thomas, J. Y. Hardberg, and O. Laligant, "Illuminant estimation in multispectral imaging," J. Opt. Soc. Am. A **34**, 1085–1098 (2017) vol 19.
[5] K. Hara, K. Nishino, and K. Ikeuchi, "Multiple light sources and reflectance property estimation based on a mixture of spherical distributions," *Proc. ICCV* (IEEE, Piscataway, NJ, 2005), Vol. II, pp. 1627–1634.
[6] A. Gijsenij, R. Lu, and T. Gevers, "Color constancy for multiple light sources," IEEE Trans. IP **21**, 697–707 (2012).
[7] Y. Imai, Y. Kato, H. Kadoi, T. Horiuchi, and S. Tominaga, "Estimation of multiple illuminants based on specular highlight detection," *Proc. CCIW, Lecture Notes in Computer Science, LNCS6626* (Springer, Berlin, 2011), pp. 85–98.
[8] S. Tominaga, T. Horiuchi, and Y. Kato, "Scene Illuminant estimation of multiple light sources," *Proc. IS&T/SID CIC20: Twenty Color and Imaging Conf.* (IS&T, Springfield, VA, 2012), pp. 47–51.
[9] P. Koirala, P. Pant, M. Hauta-Kasari, and J. Parkkinen, "Highlight detection and removal from spectral image," J. Opt. Soc. Am. A **28**, 2284–2291 (2011).
[10] R. O. Duda and P. E. Hart, *Pattern Classification and Scene Analysis* (John Wiley & Sons, New York, 1973).
[11] A. Rosedfeld, R. A. Hummel, and S. W. Zucker, "Scene labeling by relaxation operations," IEEE Trans. SMC **6**, 420–433 (1976).
[12] S. W. Zucker, "Relaxation labelling: 25 years and still iterating," in *Foundations of Image Understanding*, edited by L. S. Davis (Kluwer Academic Publishers, Boston, 2001), pp. 289–322.
[13] J. Joglekar, S. S. Gedam, and B. K. Mohan, "Image matching using SIFT features and relaxation labeling technique," IEEE Trans. GRS **52**, 5643–5652 (2014).
[14] B. Kumar and O. Dikshit, "Spectral contextual classification of hyperspectral imagery with probabilistic relaxation labeling," IEEE Trans. Cybernetics **47**, 4380–4390 (2017).
[15] S. Tominaga, K. Hirai, and T. Horiuchi, "Estimation of fluorescent Donaldson matrices using a spectral imaging system," Opt. Express **26**, 2132–2148 (2018).